Numerical investigations on winglet effects on aerodynamic and aeroacoustic performance of a civil aircraft wing

Erfan Vaezi[*1] and Mohammad Javad Hamedi Fijani[2a]

1Department of Aerospace Engineering, Sharif University of Technology, Azadi Ave, Tehran, Iran
2Department of Mechanical Engineering, University of Windsor,
401 Sunset Ave, ON N9B 3P4, Windsor, Canada

Abstract. The paper discusses the effect of the winglets on the aerodynamic and aeroacoustic performance of Boeing 737-800 aircraft by numerical approach. For this purpose, computational fluid dynamics and fluent commercial software are used to solve the compressible flow governing equations. The RANS method and the K-ω SST turbulence model are selected to simulate the subsonic flow around the wing with acceptable accuracy and low computational cost. The main variables of steady flow around the simple and blended wing in constant atmospheric conditions are computed by numerical solution of governing equations. The solution of the acoustic field has also been accomplished by the broad-band acoustic source model. The results reveal that adding a blended winglet increases the pressure difference near the wingtip, which increases the lift force. Also, the blended winglet reduces the power and magnitude of vorticities around the wingtip, which reduces the wing's drag force. The effects of winglets on aerodynamic forces lead to a 3.8% increase in flight range and a 3.6% increase in the maximum payload of the aircraft. Also, the acoustic power level variables on the surfaces and fields around the wing have been investigated integrally and locally.

Keywords: aerodynamic performance; aircraft acoustic; blended wing; commercial aircraft; numerical simulation

1. Introduction

For more than 60 years, researchers have been aerodynamically optimizing their designs not only in the aerospace field but also in other areas, including turbines, bridges, and a variety of vehicles (Skinner and Zare-Behtash 2018). Thus, major aircraft companies meditate to increase their products' operational efficiency with flight range, fuel consumption, and payload capacity for more portions of the aviation market. For this purpose, two methods of experimental tests and numerical simulations are available for researchers (Rubbert 1990). According to dimensions, the expensiveness of wind tunnel tests, frequent geometric corrections, and time-consuming manufacturing processes caused computer simulations' popularity with appropriate accuracy, high speed, and low cost (Ortiz *et al*. 2002). From the appearance of numerical methods – based on the

---

∗Corresponding author, Master's Student, E-mail: erfan.vaezi@ae.sharif.ir
ª Master's Student, E-mail: hamedif@uwindsor.ca

discretization of partial differential governing equations – engineers try to utilize the methods in their research fields.

In the field of the use of numerical methods for aerodynamic topics, several papers have been published. Effective implementation of numerical methods for aircraft analysis has an essential role in the design process (Tinoco 2007). In this area, Hasanzadeh *et al*. (2012) studied ice formation on an airfoil and its effects on the wing performance for various angles of attack. In this paper, a combined method contains a multi-block Navier-Stokes equations code, boundary layer method, and panel theory used for numerical modeling of the control volume. They noticed that the stall angle is 12º for an icy wing while the typical wing is around 16º. In another study, Dziubinsky *et al*. (2016), Simulated flow-field around an agricultural aircraft with RANS formulation and two turbulence models of k-ω SST and Spalart-Almaras. They calculated the aerodynamic features of aircraft for various flight conditions by a steady-state approach. They compared them with the available experimental results to investigate dust propagation effects on the performance. They mentioned that according to the accuracy of k-ω SST in the boundary layer, it has more accuracy to simulate separation point and stall angle. In the paper of Ghoreyshi *et al*. (2010), the feasibility study of Ranger 2000 fighter maneuvers was studied using numerical aerodynamic data. To do so, they used an upgraded numerical code at the University of Liverpool called PMB (Parallel Multi-Block). This code solves discrete Euler and RANS equations with a finite volume approach on a multi-block grid. It calculates aerodynamic force and moment coefficients based on solving the unsteady flow. At first, they collected several conventional flight maneuvers of the mentioned fighter and, by Table Generation methods, identified several different positions in terms of variables such as angle of attack, side-slip angle, and control surfaces deflection. Two grid modification methods, including rigid motion and transfinite interpolation, were used to accurately predict control surfaces' movement during the maneuver. The data needed for the tables were completed. Finally, while validating the results with experimental data, they stated that for the studied maneuvers. However, the application of the numerical method is sufficiently accurate. In order to understand this method's limitations, it is necessary to examine more maneuvers.

Commercial software is one of the standard tools which is used to simulate and study fluid flow. Implementing a successful numerical simulation requires prerequisites, which are shown in Fig. 1 (Tinoco 2007). According to recent developments in computational systems, various research studies have been done to study aircraft performance by common CFD tools (Tinoco 2007). Lazim *et al*. (2003) studied subsonic flow around a fighter with an external tank on the wing by Fluent software. In this paper, the comparison of numerical results and experimental data are acceptable according to maximum pressure distribution, in which the error reported around 19%. They also found that the external tank's effect depends on the aircraft's speed and is limited to the wing's lower surface. Triet *et al*. (2015) simulated flow around NACA 2412 airfoil to find lift and drag in various airspeeds between 0 up to 50 m/s by fluent. In their research, the maximum value of the lift-to-drag ratio was reported as 22.5. According to numerical results, they calculated stress distribution on the wing and offered operational data for the initial design of unmanned aircraft. Hiremath and Malipatil (2014) studied flow around a Boeing 777 at a constant speed and various angles of attack between 1.5º and 18º by CFX software. Their results were compatible with fundamental theories of wing aerodynamic. Fillola *et al*. (2004) analyzed flow around control surfaces by a numerical approach. They use an adjustable method of grid generation to improve the accuracy of the solver. Also, they studied the effects of ailerons by a piecewise and deformable computational grid. Besides, the drag force coefficient and hinge moments of the aileron were
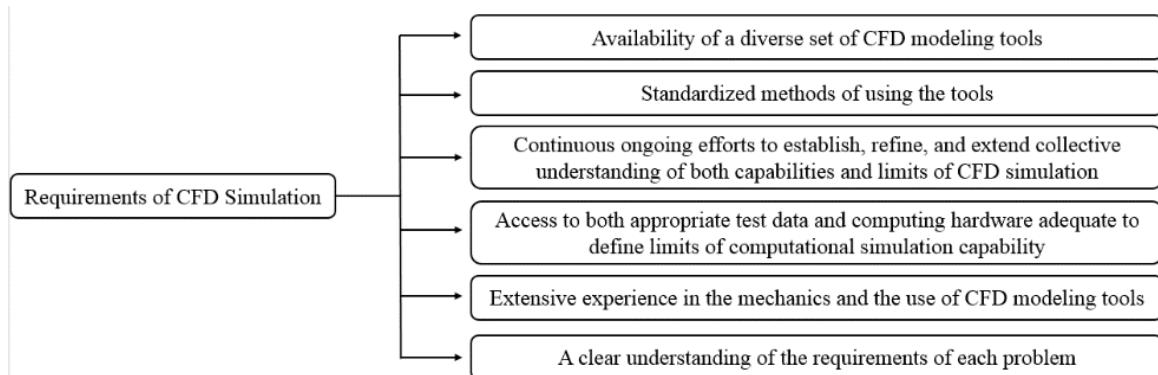
Fig. 1 Requirements of Successful CFD Simulations (Tinoco 2007)

Table 1 Summary of researches in the field of aerospace using computational fluid dynamics method

Sources	Methods	Geometry	Purpose of the study
Hasanzade *et al.* (2012)	CFD code	Wing	Changes in stall angle due to various ice formation on a wing
Dziubiński *et al.* (2016)	Fluent	Agricultural aircraft	Agricultural dust effects on aircraft performance
Ghoreyshi *et al.* (2010)	PMB Code	Fighter aircraft	Different flight maneuvers
Lazim *et al.* (2003)	Fluent	Fighter aircraft	Effect of the tank installed under the wing
Triet *et al.* (2015)	Fluent	Airfoil	The effect of the angle of attack on the lift and drag forces
Hiremath *et al.* (2014)	CFX	Passenger aircraft	The effect of angle of attack on aircraft aerodynamics
Fillola *et al.* (2004)	elsA	Control surfaces	The effect of control surfaces geometry on forces and torque of the hinges
Shankara *et al.* (2012)	STAR-CCM+	Trapezoidal wings	The location of boundary layer transition on the wing

calculated for 0º, 25º, and 45º angles of attack.

Shankara and Snyder (2012) performed the numerical simulation of the flow around a high-lift trapezoidal wing. They modeled the steady flow using the RANS formulation and the K-ω SST turbulence model by STAR-CCM + software. The flow around the wing is in the subsonic flow regime with a temperature and pressure of 520 R and 1 atm. They set their goal to determine the transition point of the boundary layer flow regime on the wing from laminar to turbulent. To do so, they coupled their original turbulence model with the laminar-to-turbulence transition model. Finally, while validating their results with experimental data related to the lift and pressure coefficients, they calculated the transition of the boundary layer flow regime on the wing in terms of the angle of attack. Table 1 summarizes the previous research reviewed in this article.

Another practical aspect of commercial software is the calculation of the acoustic field of fluidic physics. One common area is aeroacoustics, which is examined by a steady and unsteady flow solution. Although the acoustics of flow due to pressure fluctuations over time is an unsteady phenomenon (Tam 1995), it can be calculated with some models such as broadband noise source.

On the other hand, it is anticipated that noise reduction is one of the main issues considered in the next generation of aircraft design. Also, due to the ease of using numerical methods in the early stages of design, computational aeroacoustic analysis methods will be highly regarded (Ewert *et al*. 2011). Sometimes in the final stages of aircraft design, especially pre-construction optimizations, aeroacoustics is also tested experimentally (Czech *et al*. 2012). However, a significant number of numerical research in the field of aeroacoustics has been published. In the paper of Lefebvre *et al*. (2010), the propeller optimization of a light aircraft was investigated. This research is part of a French project called ANIBAL, which was launched in recent decades to improve the acoustic performance of propellers (Lefebvre *et al*. 2010). The main optimization constraints, including usability in light aircraft such as the Robin DR 400-180 and the reduction of at least 5 dB of noise generated, were defined. Also, to improve acoustic performance, the propeller had to maintain its aerodynamic aspects. For this purpose, elsA numerical software was used to simulate the field, and flight tests were used to observe its performance practically. In their paper, they stated that the final model was able to reduce the noise generated by the propeller by 9 dB. Mahmoudi *et al*. (2012) studied the sound generated by the nozzle output of an aircraft engine in Fluent software. They calculated the generated sound of the engine to the aircraft surfaces by simulating the flow at altitudes of 4×10^3, 8×10^3, and 1.2×10^4 m by using the broadband noise source model.

Pagano *et al*. (2008) worked on the multi-objective optimization of a light aircraft propulsion system in the same context. They expressed that in addition to propeller geometry, aerodynamic performance is also effective to generated noise. So, they examined the optimization of the planform and the number of propellers. Their study was performed numerically with the coupled Fluid-Structural Interaction (FSI) and aeroelasticity methods. Then, they implemented the numerical results in a multi-objective optimization method and defined the main constraints as noise reduction in the take-off stage and preserve propeller efficiency in cruise flight. They considered the sharp increase in propeller noise at the take-off phase due to the flow unsteadiness of non-cruise flight. They considered preserving aerodynamic performance in cruise flight as the main factors by defining the above constraints. Their results illustrated that using a multi-objective optimization algorithm to modify the planform will lead to a reduction of 1.5 dB, and the use of a 6-bladed baseline propeller system instead of 5-bladed will reduce 2 dB of generated noise. In a paper by Chae *et al*. (2010), the geometric optimization of a helicopter rotor to improve the aeroacoustic performance of the hover phase was investigated. Their analysis was based on the coupling of Kirchhoff methods and computational fluid dynamics and was considered to optimize the kriging-model-based genetic algorithm. Their CFD solver solves the flow field based on 3D Euler equations around the rotor and provides the necessary information for calculating the Kirchhoff model. Their results showed that better geometry is produced by using airfoil transition and an autorotation index in terms of reduction in High-speed impulsive noise, and the isodynamic performance of the rotor is maintained.

In a paper by Nardari *et al*. (2019), the generated noise of a UAV propeller was investigated experimentally and numerically. This research simulated the flow field numerically using SIMULIA PowerFLOW software and the Lattice-Boltzmann method to compare with the experimental results. The performance of the UAV is examined in static thrust, and by being located in the center of the room, then the generated noise is measured at different internal points. Their results illustrated that the interaction of the propeller leading edge with the vorticity caused by the vortex flow is one of the main factors in the unstable loads' production in the field, which will lead to significantly higher blade passing frequency harmonic peaks. Imamura *et al*. (2010)

studied the aerodynamics and acoustic field of a landing gear. The landing gear is a 2-wheeler and belongs to the 100-seat aircraft, which has been numerically checked with two different numerical codes. The first numerical code is appropriate for the unstructured computational grid, and by that, the aerodynamic properties of the model are adapted to the steady-state. The second code is suitable for the structured computational grid and has a higher accuracy with which the flow in the transient state is solved. The Williams and Hawking acoustic model was also used to calculate the acoustic field. In a part of their results, while comparing the available numerical and experimental acoustic data, the accuracy of the so-called model for use in the flow around the landing gear and its acoustic estimation was investigated.

Numerical aeroacoustics is commonly used in many academic and industrial types of researches. For example, in a paper by Mohamud and Johnson (2006), the use of numerical methods to solve acoustic fields in the HVAC field was validated. They selected two aeroacoustic numerical models based on Lighthill acoustic analogy. Their numerical models are Broadband Noise Source (BNS) and are known as Proudman and Carl models. They used these tools to redesign an automotive HVAC center duct with high levels of NVH. During this research, the design process was performed based on the mentioned models, and after manufacturing the device, they compared the numerical and experimental results with each other. Finally, they concluded that BNS models are a reliable method to calculate the acoustic field in the design and pre-construction process. In another paper, Li *et al.* (2010) examined the noise generated by a turbocharger numerically. In this paper, the broadband noise source model is used to study the effect of input geometry variables, blade shape, and different clearances between casing and impeller on the flow field. Their results showed that the highest values of static pressure and sound power were near the output of the impeller, and on the other hand, the noise level in terms of cylindrical and conical inlets will be less than other geometries. In a paper by Horváth and Vad (2009), they investigated the aeroacoustic field of a fan by numerical simulation and broadband noise source model. The studied fan was in an unskewed datum case and forward skewed case, and the purpose of the simulation was to find the geometry with less noise. They used Fluent software to apply the broadband noise source model to the field, claiming that the latter, besides higher aerodynamic efficiency, also performed better acoustically. Also, in the abstract of their paper, they stated that the use of the above aeroacoustic model has acceptable accuracy in studying the acoustic of the fans.

Tsai *et al.* (2009) investigated the effect of the spoiler and endplate installation on the performance of a passenger car. For this purpose, they used Fluent software to simulate the flow field and investigated the effect of these two external surfaces on aerodynamic and acoustic performance. Their numerical solver was adjusted with RANS, k-ω SST, LES turbulence model, and Ffowcs Williams and Hawking acoustic model. Their results showed that the spoiler reduces the lift force of the car, and the endplate also reduces the noise produced by the car. They also examined five different geometries for the external surfaces and compared their performance with and presented the optimal geometry. Minelli *et al.* (2020) studied aerodynamic and aeroacoustic variables around a high-speed train. According to previous studies, they have detected the front part of the train, including the bogie cavity, as the primary source of noise pollution. The study of its acoustic field is essential in densely populated areas. Then, by STAR-CCM+ software, they identified the relationship between the noise generation mechanism and the flow, then considered the two main aerodynamic structures near the body and the ground as the main factors of noise generation. Finally, while comparing their numerical results with the available experimental results, they also presented a set of new acoustic data for this train. Table 2 illustrates a summary

Table 2 Summary of researches in the field of acoustics using computational fluid dynamics method

Sources	Area of study	Geometry	Purpose of study
Lefebvre *et al.* (2010)	Propeller design	Robin DR 400	Reduce generated noise of a propeller while saving aerodynamic performance
Mahmoudi *et al.* (2012)	Aircraft	Engine nozzle	Measuring generated sound of engine outlet flow at various flight altitudes
Pagano *et al.* (2008)	Propeller design	Light civil aircraft	Reduction of noise produced in the take-off while preserve aerodynamic performance of the cruise mode
Chae *et al.* (2010)	Rotor design	Civil helicopters	Improving the aeroacoustic performance of a civil helicopter rotor in terms of noise reduction in the hover phase
Nardari *et al.* (2019)	UAV	UAV propeller	Studying the generated noise by a UAV in various points of a test chamber
Imamura *et al.* (2010)	Aircraft	landing gear	Checking the accuracy of Ffowcs Williams and Hawking model for calculating the acoustic field of the landing gear
Mohamud *et al.* (2006)	HVAC	Center Duct HVAC	Feasibility study of using BNS methods in the early phases of HVAC design
Li *et al.* (2010)	Turbomachine	Turbocharger	Using BNS models to study the effect of geometric variables on the acoustic field of the flow within the turbocharger
Horváth *et al.* (2009)	Turbomachine	Axial fan	Studying of noise level in 2 design modes: unskewed blade and forward skewed
Tsai *et al.* (2009)	Passenger car	spoiler and endplate	Studying the effect of spoiler and endplate on aerodynamic performance and the amount of noise produced by the car
Minelli *et al.* (2020)	Railroad	ICE3 train	Identifying the main areas of effect of the flow structure on the production of noise in the bogie cavity

of the research in the numerical calculation of the acoustic field of the flow.

One way to increase the aerodynamic performance of aircraft is to add winglets into the wingtip area to reduce the power of the generated vorticities'. That led to an increment of lift force and a decrease in drag force (Mahmood and Das 2019). In this context, Gavrilović *et al.* (2015) studied the effects of 5 different winglet configurations on the induced drag of a wing. To find aerodynamically optimized winglet geometry, they calculated aerodynamic coefficients of the wing for all winglets by Fluent. They also calculated flight range and maximum payload for each geometry and concluded binary winglet has the highest aerodynamic efficiency. Elham *et al.* (2014) used a multi-objective genetic algorithm to find the best configuration of winglets with drag reduction and minimum structure weight. Their new design led to a 3.8% reduction in fuel consumption and 29 M\$ in maintenance costs over 15 years. Jain *et al.* (2016) selected NACA 2415 as their case study to investigate the effects of winglets. They utilized the RANS formulation and Spalart-Almaras turbulence model in Fluent to simulate flow-field, constant atmospheric conditions, constant Mach number, and various angles of attack. Their calculations were compatible with winglets' primary effects, such as more stability, flight range, and less fuel consumption.

In a paper by Maughmer *et al.* (2002), an airfoil was designed and tested for use in the structure of winglets. They initially designed the airfoil to improve the performance of the winglet and named it PSU 94097. Then, to validate the performance of the airfoil, it was examined in a wind tunnel in terms of Reynolds numbers 2.4×10^5 and 1×10^6, and the flow characteristics around the

airfoil were measured using XFOIL and PROFIL numerical codes. While validating their numerical results, they considered the performance of the mentioned airfoil as a suitable cross-section for winglet design. Ali (2020) studied numerically and experimentally the effect of two models of blended and spiroid winglets on the performance of a rectangular wing. First, They simulated flow under incompressible conditions and the k-ω turbulence model using the Ansys Fluent solver. Then, by 3D printing, they made two wing models and tested them in a wind tunnel with a maximum speed of 55 m/s. Their results showed that the L/D ratio for both wings occurred at a 6º angle of attack, while the blended winglet value is about 20% higher than the spiroid. They concluded that the performance of the blended winglet enhances the stability of the wing by further increasing the pitching moment compared to the spiroid winglet. Zhang *et al*. (2020) investigated how winglet affects on solar-powered aircraft. By using multi-constraint optimization, they tried to increase the cruise time of a solar-powered aircraft. Their optimization constraints fall into four general categories, including geometry, aerodynamics, energy, and stability, which are the most critical topics in solar-powered aircraft. Although their optimized model is weaker than the original model in terms of reducing drag and structural weight, it improves aircraft performance in terms of cruise flight capability. Also, using different aspect ratios and applying the mentioned optimization algorithm, they stated that by exceeding a certain limit of the aspect ratio, the winglet effect disappears. To increase the effectiveness of winglet systems, Eguea *et al*. (2020) examined morphing winglets. They stated that fixed winglet systems performed well only in one flight mode, while the aircraft experiences different modes during a flight scenario. Using the genetic optimization algorithm, they calculated the value of the winglet span-wise camber in different flight modes in terms of changing the angle of the trailing and leading edges. They optimized results on one midsize business jet and reported that in this case, the fuel consumption is reduced by about 6% compared to the simple winglet under the same conditions.

Generally, every system that evaluates its performance based on fluid flow vorticity, has the potential to implement winglet devices. Nowadays, winglets have been widely employed in wind turbines, heat exchangers, and marine propulsive systems. So optimization of their performance based on numerical simulations is a necessity for researchers. Gao *et al*. (2019) studied six different geometry of winglets adjoin to a marine propeller. They used RANS formulation and volume of fluid (VOF) to the simulated flow field. All six geometries had the same features except the rake angle, which should be optimized according to the system's general efficiency. Besides, they noticed that winglets reduce the pressure drop in the suction area of the propeller. Farhan *et al*. (2019) investigated the effects of winglet geometry on reducing wingtip vortices of the wind turbine. Firstly, they validated the numerical solver with available experimental data and then introduced a 15 cm rectangular winglet with a 45º conical angle as the optimum design. Kobayashi *et al*. (2019) studied the potential effect of winglets on a low Reynolds heat exchanger. Performance optimization is done by testing winglets in certain positions. According to the results, their design enhanced the total heat transfer rate, and a 16% increment in the quality factor of the heat exchanger (j/f) corresponded to the previous design. Table 3 summarizes the classification of non-aerospace applications of the winglet.

One new application of winglets is in a novel transport system, which is named the aero train. There is a vertical surface at the wingtip in this vehicle, which behaves similarly to the winglets. Takoma *et al*. (2003a) studied flow around an aero train wing. They simulated flow by Ansys Fluent & Structural and expressed that the structure of subsonic flow around aero train and aircraft are entirely different, according to the ground effect's existence. Also, various parameters contain side wing direction, separation point, downwash, and wingtip vortices that affect the flow field.

Table 3 Summary of researches on the application of winglet for other systems

Source	Application area	Tools	Purpose of the study
Gao *et al*. (2019)	Marine propulsion	STAR CCM+	Investigation on different winglets to be installed on submarine propellers
Farhan *et al*. (2019)	Wind turbine	Fluent	Use proper geometry at the tip of the blades to reduce the vortices at the tip
Kobayashi *et al*. (2019)	Heat exchanger	COMSOL	Optimizing the performance of a heat exchanger by adding a winglet at a low Reynolds number
Yoon *et al*. (2003)	Aero-train	Fluent	Studying the flow around an aero train and comparison with the subsonic flow around the wing of an aircraft
Page (2000)	Racing car	CFD code	Improving the aerodynamic performance of a race car by modifying the geometry of the surfaces
Barakos *et al*. (2013)	Helicopter	Review	Investigating the effect of winglet in the design of helicopter rotor tip
Ye *et al*. (2015)	Axial fan	Fluent	Studying seven different blade tip geometries in terms of modal, aerodynamic and acoustic performance

The winglets are also applicable to use in race cars. Many car designers use winglets as a plugin to the main body to increase the competitiveness of their products. Page (2000) tried to improve the performance of a race car by various geometric modifications. Besides other geometrical modifications, a winglet device was installed in the middle part of the car to decrease the negative effects of the generated vortices. Another aerospace application of winglets is in the rotor blade tip design. A hover and forward flight combination make the helicopters one of the most versatile transport systems (Brocklehurst and Barakos 2013). In the review paper of Brocklehurst and Parakos (2013), various geometries for the blade tip design of the helicopters were discussed. Ye *et al*. (2015) examined the effects of blade tip design on the OB-84 axial fan performance. This research studied the efficacy of 7 different concept designs for blade tips. They simulated different aspects of the axial fan performance containing fluid flow, acoustic domain, and vibrations by the Ansys package. According to the results, they expressed blade tip design has significant effects on the axial fan total efficiency, which can be increased by up to 1.07%.

In several recent papers, the winglet cant angle and its dependency on the angle of attack have been examined. Thus, the cant angle has an optimum value according to the angle of attack. In this context, Myilsamy *et al*. (2015) studied the cant angle of a winglet in a commercial aircraft by AcuSolve Software. They investigated cant angles of 0º, 30º, and 90º for angles of attack between -2º and 10º. According to results, for winglets, maximum efficiency should define a direct relation between cant angle and angle of attack. In other words, more significant angles of attack should increase the cant angle, too. Helal *et al*. (2016) used Fluent to investigate the effects of cant angle on a wing based on NACA 65-218 airfoil. Fluid flow was defined in sea-level condition and 0.2 Mach number. They noticed that winglets could increase L/D ratios between 6 and 15 percentages, according to the cant angle and angle of attack. Also, they presented tables dedicated to showing optimum cant angles for every angle of attack. In another paper, Azlin *et al*. (2011) did a similar simulation for NACA 65-218 airfoil and claimed that 45º state has the most aerodynamic efficiency between several cant angles. Also, the L/D ratio's slope factor increased by about 8% compared to a simple wing.
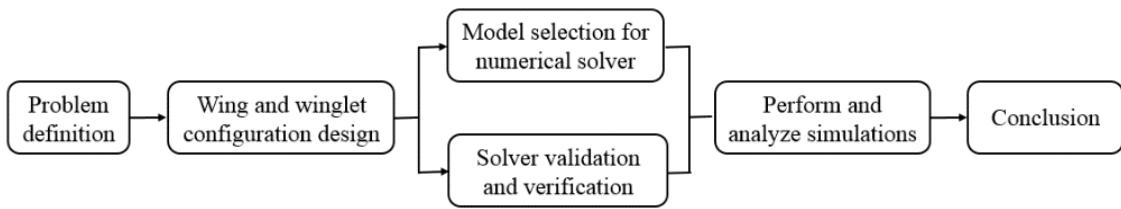
Fig. 2 Research roadmap to investigate the effects of winglet on wing's performance

In a paper, Abdelghany *et al*. (2016) examined three different winglet cant angles on the wing of a Cessna aircraft model with a NACA 2412 airfoil. They compared the angles of 0º, 30º, and 45º of the winglets with the winglet-less wing, using Fluent software. The flow regime was subsonic, and sea-level atmospheric conditions were applied. The initial part of their results included expressing the main effects of winglets on flow physics and results such as increasing the lift force and decreasing the drag coefficient. They further stated that the maximum increase of lift coefficient and decrease of the drag coefficient was equal to 12% and 4%, respectively. In the end, they concluded that by increasing the cant angle from 0º to 45º, the performance of the winglet is also improved so that the best aerodynamic efficiency is related to the 45º mode. In a paper by Guerrero *et al*. (2020) investigated the effect of two geometric variables, cant angle and sweep angle, on the performance of the winglet mounted on the wing of the Onera M6. The simulation of the subsonic flow regime according to Mach numbers 0.3 and 0.839 was performed using Ansys Fluent software. Different values were considered for sweep angles equal to 30º, 45º, and 60º and cant angle equal to 0º, 15º, 45º, and 80º. Their results showed that changing the conical angle did reduce the stall angle, while $C_{L,max}$ value, decreases with high cant angles. They also stated that high sweep angles improve aerodynamic performance due to the reduction of drag force and wave drag at higher Mach numbers.

The primary purpose of this paper is to investigate the effects of winglets by the aerodynamic and aeroacoustic approach to achieve a complete apprehension of flow-field around the wing. As far as we know, previous research in this field has been mainly in the form of case studies with a limited aerodynamic approach, and comprehensive research has not been done to find out the effect of winglet aerodynamics and aeroacoustics. This purpose has been followed by the computational fluid dynamics method and Fluent software. RANS method was used for the formulation of the governing equations, which is a common tool for aerodynamic studies (Jameson and Fatica 2006). This paper discussed the main aerodynamic parameters at a constant speed and various angles of attack. Also, based on aerodynamic performance, flight features, including range and maximum payload, have been examined. Also, the acoustic field is calculated by numerical solution of the control volume and broadband noise source model. Thus, the acoustic power level of different surfaces and points has been discussed. Fig. 2 shows the roadmap of the research.

2. Governing equations and numerical solution method

In this section, governing equations of fluid flow are introduced, then turbulence and acoustic models applied for the domain are discussed. The model used to simulate the steady acoustic field is also briefly introduced. Attempts have also been made to express the scientific basis for using each model to verify the numerical solution method.

2.1 Flow governing equations

For the current study, fluid flow is defined as compressible and subsonic. Primary governing equations of fluid flow contains continuity, linear momentum conservation, and energy conservation are defined as Eq. (1) in the vector form (Moayyedi 2016):

$$\frac{\partial Q}{\partial t} + \frac{\partial E}{\partial x} + \frac{\partial F}{\partial y} + \frac{\partial G}{\partial z} = 0 \tag{1}$$

where the vectors are defined as below:

$$Q = [\rho \quad \rho u \quad \rho v \quad \rho w \quad \rho e_t]^T \tag{2}$$

$$E = \begin{bmatrix} \rho u \\ \rho u^2 + p - \tau_{xx} \\ \rho uv - \tau_{xy} \\ \rho uw - \tau_{xz} \\ (\rho e_t + p)u - u\tau_{xx} - v\tau_{xy} - w\tau_{xz} + q_x \end{bmatrix} \tag{3}$$

$$F = \begin{bmatrix} \rho v \\ \rho vu + p - \tau_{yx} \\ \rho v^2 + p - \tau_{yy} \\ \rho vw - \tau_{yz} \\ (\rho e_t + p)v - u\tau_{yx} - v\tau_{yy} - w\tau_{yz} + q_y \end{bmatrix} \tag{4}$$

$$G = \begin{bmatrix} \rho w \\ \rho w - \tau_{zx} \\ \rho wv - \tau_{zy} \\ \rho w^2 + p - \tau_{zz} \\ (\rho e_t + p)w - u\tau_{zx} - v\tau_{zy} - w\tau_{zz} + qz \end{bmatrix} \tag{5}$$

In Eqs. (2)-(5), ρ is density, u, v, and w are velocity components in the Cartesian coordinate system. Various components of Reynolds stress are shown as τ_{ij}, static pressure as p, and heat flux parameters as qi. The flow equations are solved by RANS (Reynolds-Averaged Navier-Stokes) method. This method has a high potential for accurate calculation of turbulent flows with low computational cost, so it is suitable for the numerical formulation of this study (Diskin and Thomas 2016). Also, using this formulation, along with turbulence models, is a critical tool equation in aerospace design and studies (Park *et al*. 2018).

2.2 Equations of the turbulence model

Using different models of k-ω models is common to simulate flow around aerospace vehicles (Dziubiński *et al*. 2016). To calculate turbulence effects in the control volume, the k-ω SST model has been used, which is a two-equation eddy viscosity model. Features of this model in the internal part of the boundary layer led to an appropriate performance in the viscous sub-layer. Also, it is used as a low Reynolds turbulence model without an additional damping function. On the other hand, the k-ω model has similar behavior for the fluid flow compared to k-ε, but they do not have

problems with the k-ε model in simulation of the inlet flow turbulence features (Moayedi and Mohammad 2019). Also, k-ω SST has an accurate performance to simulate separation flow and inverse pressure gradient (Dziubiński *et al*. 2016). The k-ω SST model equations for compressible flow are as follows (Wilcox 1998):

$$\frac{\partial(\rho k)}{\partial t} + \frac{\partial(\rho u_j k)}{\partial x_j} = H + \frac{\partial}{\partial x_j}((\mu + \frac{\mu_t}{\sigma})\frac{\partial k}{\partial x_j}) \tag{6}$$

$$\frac{\partial(\rho \omega)}{\partial t} + \frac{\partial(\rho u_j \omega)}{\partial x_j} = H + \frac{\partial}{\partial x_j}((\mu + \frac{\mu_t}{\sigma})\frac{\partial \omega}{\partial x_j}) \tag{7}$$

where k is turbulent kinetic energy, ω is turbulent dissipation ratio and H, which is a combination of density, static pressure, and constant values. Also μ_t is turbulent viscosity, which is calculated as Eq. (8):

$$\mu_t = C_\mu f \frac{k}{\omega} \tag{8}$$

2.3 Equations of the acoustic model

In this section, Broadband noise source model equations are examined where extracted from Lighthill equations. Proudman used the results of Lighthill's research to find acoustic power generated by homogenous turbulence without mean flow as Eq. (9) (Mahmoudi 2012). As flow simulation is done steadily, broadband noise source model used where calculated acoustic field without temporal pressure fluctuations. Also, this model has convergence with k-ω SST in RANS formulation, which led to acceptable accuracy in a steady-state flow field (Pietroniro *et al*. 2018). The primary advantage of this model is its accurate recognition of noise sources, and the main drawback is the inability of the model to calculate the frequency (Pietroniro *et al*. 2018). In Eq. (9), P_A is acoustic power in volume unit, u is turbulent velocity, ℓ is specific length, a_0 sound of speed, and α is a constant coefficient. Then P_A is used to find acoustic power as below:

$$L_P = 10\log(\frac{P_A}{P_{ref}}) \tag{9}$$

where L_P shows acoustic power in decibel, P_{ref}, P_A are acoustic power in volume unit for references and desired point of A.

2.4 Geometry

In order to design wings with high aerodynamic efficiency, aerospace engineers are trying to enhance the performance by joining lift generator devices (Gavrilović *et al*. 2015). Wings with winglets are a typical design pattern for aircraft designers. Generally, winglets affect wingtip vortex, which presents operational benefits by reduction of tip vortex energy. Winglets reduce parasite and lift-induced drag and also generate extra lift by smoothing flow near the wingtip. Lift force increment not only caused by smoothing the flow but also by additional generated lift on the winglet. The winglet used the wingtip vortex rotational flow to generate lift. The increase of winglet effect with the angle of attack is due to the increased lift force and, consequently, the
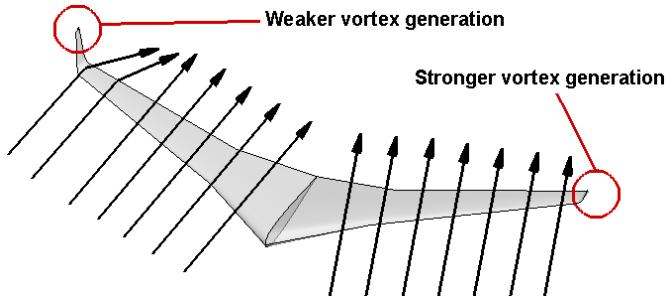
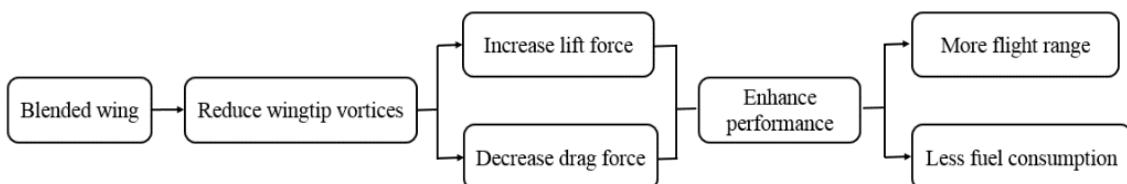Fig. 3 Main effects of winglet configuration on the streamlines

Fig. 4 Schematic diagram of how winglet affects performance

Table 4 Geometric specifications of wing section

Parameter	Value
Sweep Angle (º)	25.02
Mean Aerodynamic Chord (m)	3.96
Wingtip Chord (m)	1.25
Wing Root Chord (m)	7.88

Table 5 Geometric specifications of wing

Parameter	Value
Taper Ratio	0.16
Aspect Ratio	9.45
Area (m^2)	124.6
Dihedral Angle (º)	6
Wing Span (m)	34.32

stronger vortex wingtip. Fig. 3 shows the effect of the winglet on the wingtip vortex.

Several geometries have been used for winglet design yet, but the most common winglet configuration for commercial aircraft is blended type. Despite multiplicity winglet geometries, their operation and function are similar. Their primary effect is the reduction of wingtip vortices so that they improve the lift and drag forces of the wings (Sadraey 2012). Fig. 4 summaries how winglet affects aircraft performance.

In the current study, the wing of Boeing 737-800 was investigated in simple and blended states, According to Fig. 3. Since the difference between the two geometries is limited to the presence of the winglet, the characteristics and shape of the airfoil and wing geometric dimensions are the same in the two geometries, which are shown in Tables 4 and 5, and Fig. 5, respectively.

Fig. 5 Geometry of simple and blended wing of Boeing 737-800 aircraft
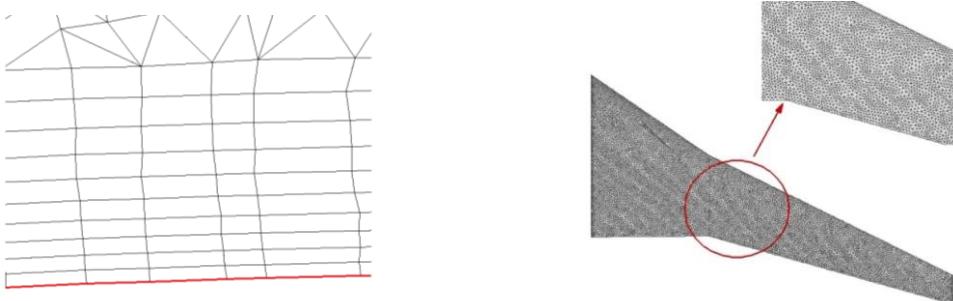

Fig. 6 Computational grid around wing (left) and on the wing surface (right)

Table 6 Computational grid information

Parameter	Value
1st Boundary Layer Thickness (m)	0.01
Height Ratio	1.1
Number of Layers	10
Total Number of Elements	1058672

2.5 Computational grid

According to Fig. 6, the computational grid has been generated after model design. Concerning the complexity of geometry and the necessity of high accuracy in calculating aerodynamic coefficients, a hybrid mesh has been used, containing structured mesh around the wing and unstructured form outside of the boundary layer. Also, to find the optimum number of elements, the mesh study process has been done. Table 6 shows the information on the final computational grid used for numerical simulations.

2.6 Boundary conditions and numerical scheme

Fig. 7 shows boundary conditions applied for numerical analysis. Pressure far-field boundary condition has been applied for the inlet boundaries of the control volume. Also, these boundaries are far enough from the aircraft until the floating object's effects are negligible on them. Adiabatic wall applied for wing surface and symmetry condition selected for side boundary of the domain. Flow field equations are discretized by the 2nd order central and with Pseudo transient formulation method. Besides, kinetic energy and turbulent dissipation rate equations are examined by the power-law scheme. Also, to calculate the changes of the separation function, the 1st order method and for the spatial discretization of the gradient, the least-squares cell-based method is used, which has a good performance for calculating the acoustic field (Ansys Inc. 2011).
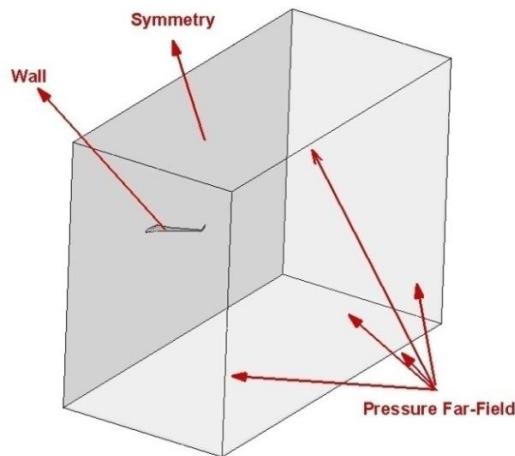
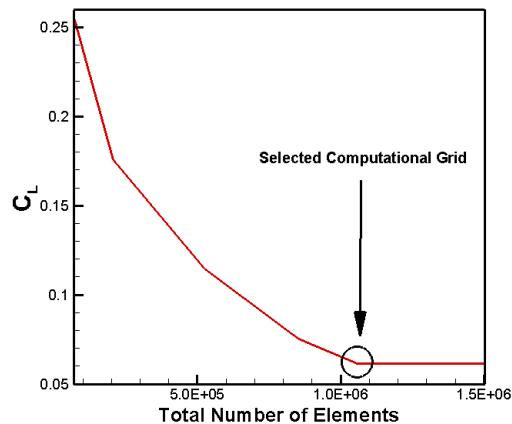Fig. 7 Defined control volume and applied boundary conditions

Fig. 8 Changes in lift force coefficient in terms of number of elements and the selected computational grid

3. Validation

As there is no appropriate experimental data for this specific case study, indirect methods are applied to validate the numerical solver. Generally, the validation process is done in the following steps:

   • Checking the sensitivity of the results to the size of the computational grid
   • Calculating the average value of y+ within the control volume and evaluate the value
   • Assessing the accuracy of the solver on geometries close to the present study

Fig. 8 shows the lift force coefficient values in terms of the total number of elements. According to the figure, the selected grid has similar accuracy with finer grids, so it has enough accuracy for the applied solver in terms of the element size. Therefore, the measured values for field variables, including pressure, are not a function of the computational grid size, which is applied to the control volume.

Furthermore, y+ is a crucial parameter to check the validity of the solver in Fluent. According to the k-ω SST turbulence model and the hybrid computational for modelling the control volume,

Table 7 Atmospheric conditions and Mach number of the inlet flow-field

Parameter	Pressure (Pa)	Temperature (K)	Mach Number	Reynolds Number
Value	101325	300	0.6	5.397×10^7
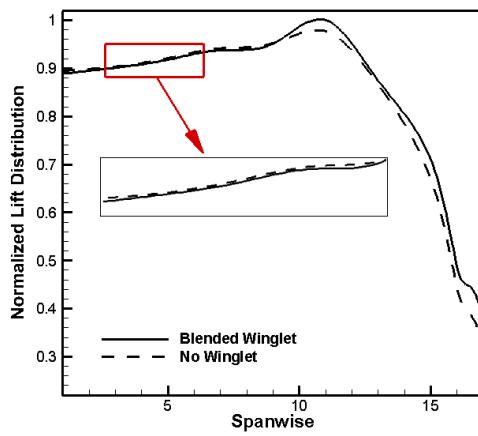
Fig. 9 Lift distribution on the simple (left) and blended wing (right) at α = 20º

y+ must be within a specific range. For this simulation, the average value of y+ for the control volume is about 0.011, which is an acceptable value for numerical simulations. Also, the final solver and computational grid are repeated in geometries close to the present study. For example, in the research of Gavrilović *et al*. (2015), the subsonic flow regime around a commercial aircraft wing under the presence of a winglet with different geometries has been investigated with Fluent software. The results related to the blended winglet indicate that the addition of the above design has improved the flight range by 3.8%. Numerical results obtained from the application of the adjusted solver in this study also show an increase of 3.77% of the flight range, which indicates a low error and accurate solver for this type of flow regime.

4. Results and discussion

In this section, various aerodynamic and acoustic parameters are examined in terms of geometric design and flow structure to analyze the wing's performance. According to Table 7, the flow field has been simulated in various angles of attack and steady-state conditions. Fluctuations of lift and drag forces and rolling moments are selected as convergence criteria, besides Fluent's primary criteria. Results are examined in several steps by quantitative and qualitative approaches. To find pressure coefficient changes in 0º, 15º, and 20º angles of attack, three sections on the wings are selected, located near the wingtip, wing root, and middle part of the wing. Also, vorticity magnitude contours near the wingtip and various angles of attack are calculated. Also, the winglet effects on the value and changes of the aerodynamic and acoustic parameters in various angles of attack are calculated to find the winglet effects on fuel consumption and performance.

Fig. 9 Shows the normalized lift distribution on the spanwise of the simple and blended wing. According to the figure, the wings have a marginal difference near the root. By approaching the tip area, the winglet effect on lift distribution is more observable, indicating that additional lift is produced near wingtip area.
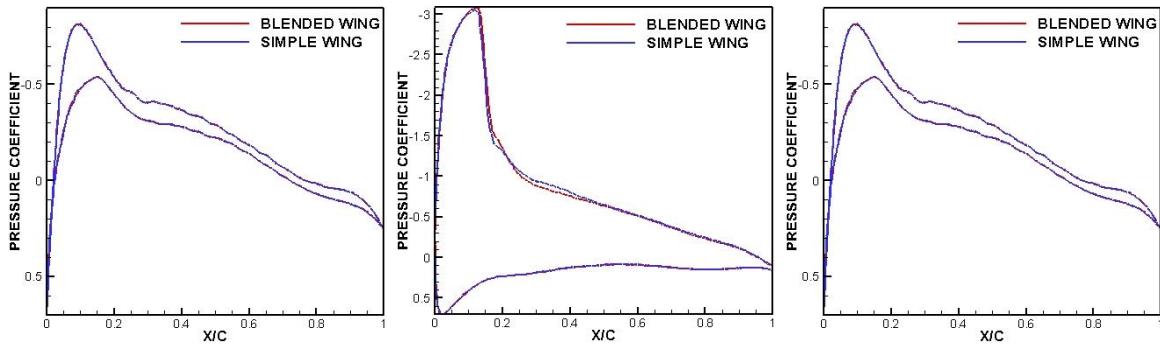
Fig. 10 Comparison of pressure coefficient distribution of simple and blended wings in 0º angle of attack for the section near wing root (left), 2nd twist location (middle), and wingtip area (right)
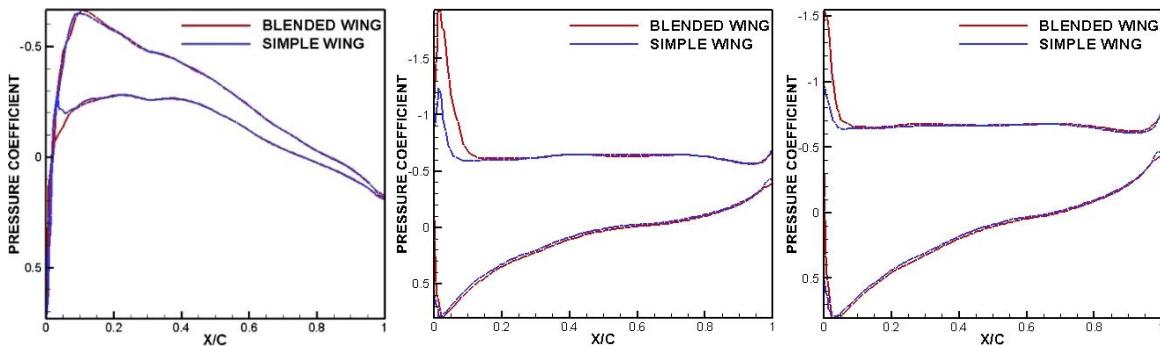

Fig. 11 Comparison of pressure coefficient distribution of simple and blended wings in 15º angle of attack for sections near wing root (left), second twist location (middle), and wingtip area (right)
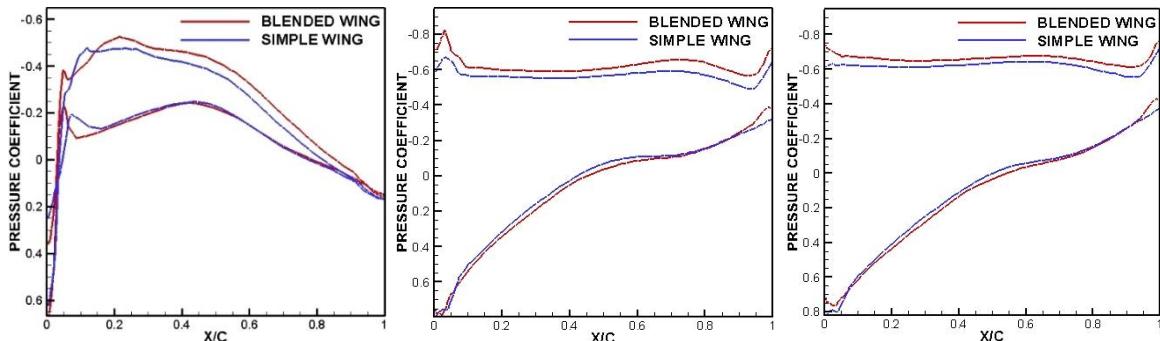

Fig. 12 Comparison of pressure coefficient distribution for simple and blended wings in 20º angle of attack for sections near wing root (left), 2nd twist location (middle), and wingtip area (right)

Figs. 10-12 show C_P distribution on three sections for 0º, 15º, and 20º angles of attack; sections have 2, 8.5, and 16.8 m distance from the symmetric plane. According to the figures, winglets reduce the induced angles near the wingtip area, increasing the C_P difference of the upper and lower surface of the wing. Generally, the figures demonstrate an increment in the winglet effects on the root by increasing the angle of attack. In fact, in cruise, the winglet does not significantly affect the root flow structure, while in the 15º, the effects are sensible, and in 20º, reach maximums

value. The 2nd section was selected in a way to be located in the middle part of the wing. According to Fig. 10, the winglet has apparent effects on the middle part, and increasing the angle of attack expands the effects from the leading edge to the whole section. In the 3rd section, the winglet affects pressure distribution utterly independent of the angle of attack.

Despite the sensible quantitative effects of winglet installation, it has a marginal influence on the pressure coefficient distribution's schematic. In fact, in most sections and angles of attack, the winglet increases the surfaces' static pressure difference by preserving the profiles. The winglet effect on the upper surface is more significant than the lower surface as in nearly all sections, the pressure distribution of the lower surface is similar for the simple and blended wing. At 0º angle of attack, the winglet has been caused a local drop-in lift force. However, in some areas, it has performed reversely. For 15º and 20º angles of attack, the winglet has a consistent effect on the wingspan to increase lift force. According to Figs. 11 and 12, at 15º and 20º angles of attack, the winglet effect extends to the wing root. Because the flow reaches the wing with a large angle of attack, the turbulence features are significant compared to the fewer angles of attack. The flow has a greater chance of transferring the winglet effects in the transverse direction. So it can be concluded that by increasing angle of attack, the winglet effects on the root will be more significant.

One of the characteristics of the winglet is its fluctuating effect on the flow around the wing at different angles of attack. As the effectiveness of winglets on the aerodynamic parameters is not constant, Eqs. (10)-(13) are used to calculate the difference percentage for various angles of attack. By these equations could reach a comprehensive analysis of the winglet effect from various angles of attack. B index is dedicated to the blended wing and S index for the simple wing in the below equations.

$$\Psi = \frac{C_{LB} - C_{LS}}{C_{LB}} \times 100 \tag{10}$$

$$\varphi = \frac{C_{DS} - C_{DB}}{C_{DS}} \times 100 \tag{11}$$

$$\chi = \frac{C_{MB} - C_{MS}}{C_{MB}} \times 100 \tag{12}$$

$$\Omega = \frac{C_{D,fS} - C_{D,fB}}{C_{D,fS}} \times 100 \tag{13}$$

Fig. 13 demonstrates the lift force coefficient of the simple and blended wing and change percentages for various angles of attack. According to the figure, the winglet has caused a marginal increment in lift force, based on the local reduction of wingtip vorticity magnitude and increment in the pressure difference between the wing surfaces. In addition to increasing the lift force coefficient at a constant angle of attack, it has also increased the wing's stall angle.

In the figure of ψ versus α, it can be seen that the percentage change of the coefficient of lift force after the initial reduction again increases to 0º angle of attack. After repeating the mentioned periodicity, it decreases continuously until it reaches the minimum value at a 15º angle of attack. From this angle of attack to the end of the graph, fewer fluctuations and more stable behavior are observed.
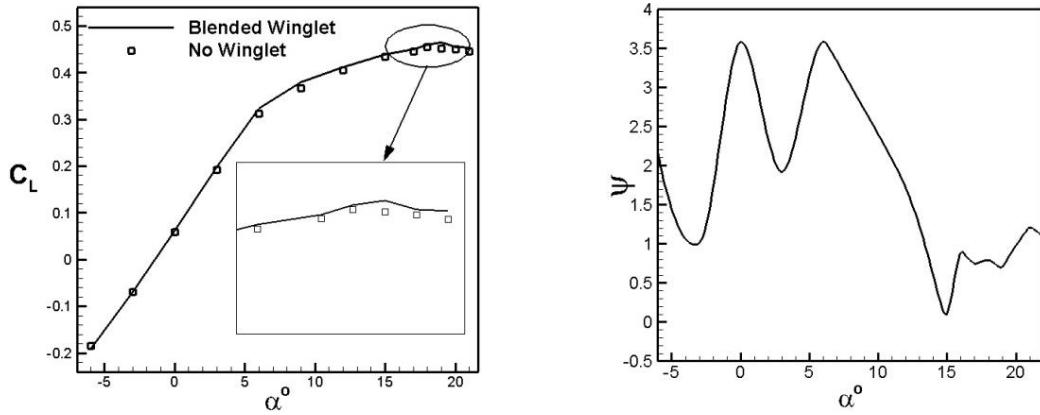
Fig. 13 Lift coefficient (left) and difference (%) (right) versus angle of attack for simple and blended wings
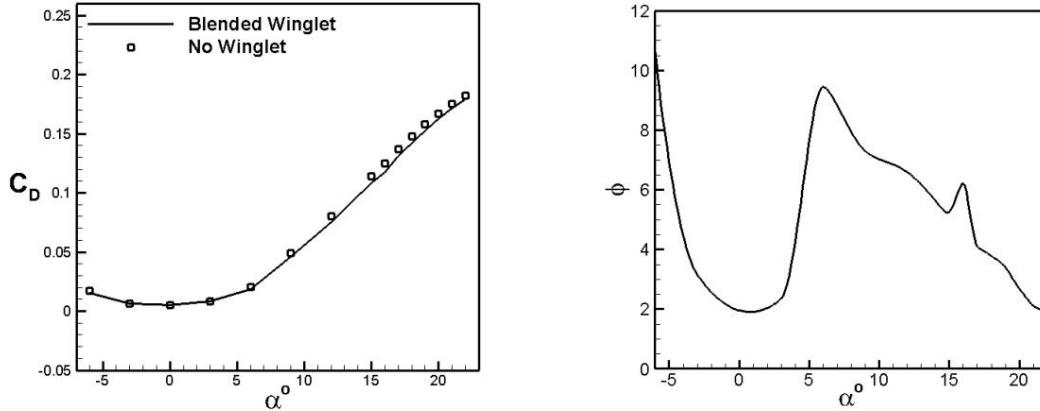

Fig. 14 Drag coefficient (left) and difference (%) (right) versus angle of attack for simple and blended wings

Fig. 14 shows the drag force coefficient of the simple and blended wings and change percentages for various angles of attack. According to the figure, the winglet installation reduces the drag force coefficient based on the reduction of wingtip vortices and the area of low pressure at the upper surface. As a result, the drag force coefficient decreases. Also, the Φ diagram shows less fluctuation in drag force coefficient behavior than the ψ diagram. It has a semi-linear schematic in negative angles of attack where only one extremum is observable for positive angles of attack, which occurs at 6º angles of attack.

Fig. 15 shows the skin friction drag coefficient value of the simple and blended wing and change percentage for various angles of attack. According to the figure, adding a winglet has increased the wetted area of the wing, which affects the skin friction drag coefficient. Also, below figures demonstrates that the increment is limited to less than 7 percent in various angles of attack.

Fig. 16 demonstrates the pitching moment coefficient value of the simple and blended wing and change percentage for various angles of attack. According to the figure, winglet installation improves the wing's longitudinal stability, especially at higher angles of attack. Also, χ has a continuous increment for the negative angles of attack. However, by reaching its maximum value
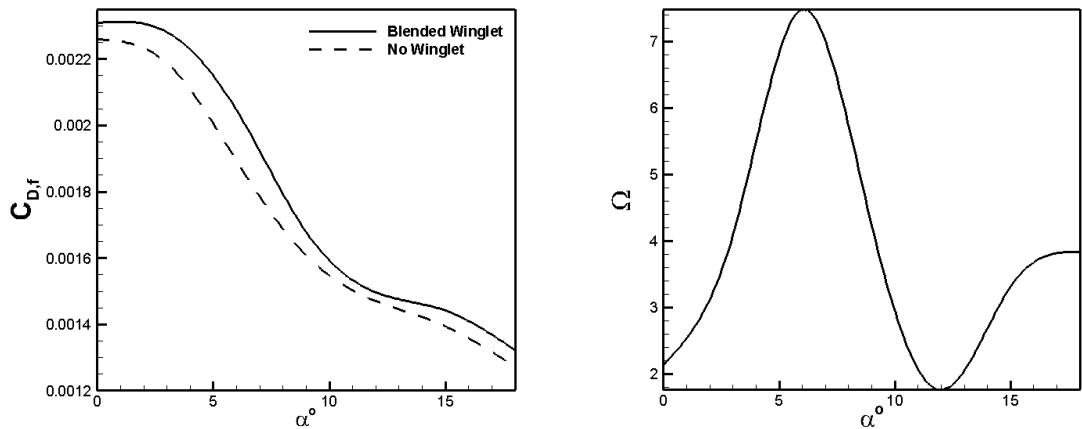
Fig. 15 Skin friction CD (left) and difference (%) (right) versus angle of attack for simple and blended Wings
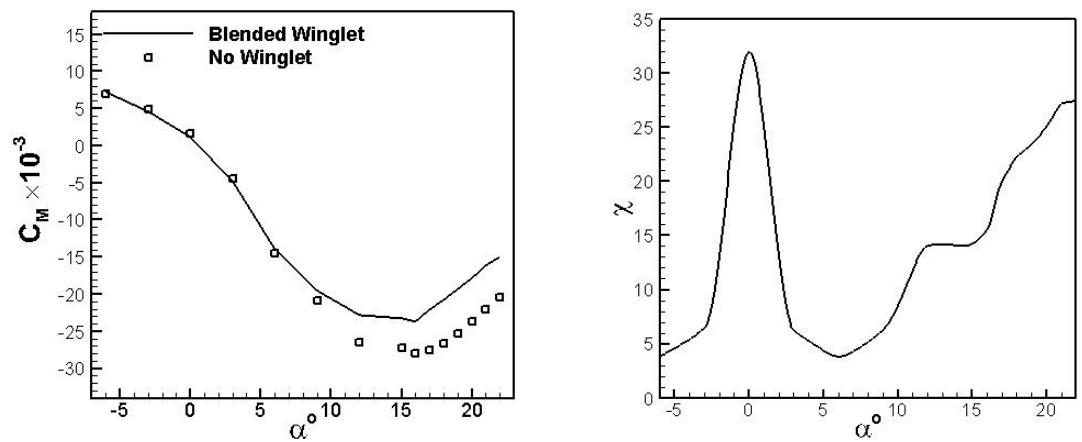

Fig. 16 Pitching coefficient (left) and difference (%) (right) versus angle of attack for simple and blended Wings
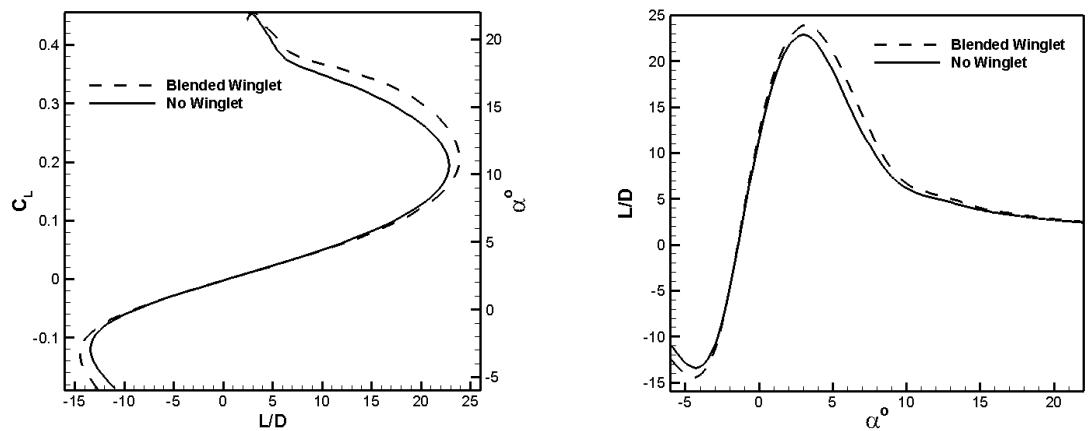

Fig. 17 Lift coefficient versus L/D and angle of attack (left) and L/D versus angle of attack (right) for simple and blended Wings

Table 8 Aerodynamic force coefficients of simple and blended wings

Wing type	Lift coefficient	Drag coefficient
simple	0.0592	0.0051
blended	0.0614	0.005

at the cruise mode, it starts to decrease and continues until the 6º angle of attack. Then it rises again with a nearly constant slope until it reaches the wing's stall angle of attack. On a swept-back wing, the additional lift on the tip due to the winglet results in a more negative pitching moment since there is additional lift force behind the wing aerodynamic center.

Fig. 17 illustrates the diagrams of lift coefficient versus L/D in various angles of attacks and L/D versus angle of attack for the simple and blended wing. According to the figure, in low and positive angles of attack, the performance of the simple and blended wings are similar, and the diagrams show marginal differences. By the increasing angle of attack to higher values, the maximum difference is observable at the 6º angle of attack. Finally, higher angles of attack present the difference is getting lower, gradually.

Despite the marginal effects of the winglet on the aerodynamic forces, it significantly influences the flight and performance parameters such as flight range, fuel consumption, and maximum payload. Table 8 shows aerodynamic forces coefficients of the simple and blended wing in the cruise mode. According to the data and equation (14) could calculate change percentage of flight range, which illustrates a 3.8% increment for the blended wing compared with the simple wing.

$$R = 2\sqrt{\frac{2}{\rho S}}\frac{1}{e_r}\frac{C_L^{0.5}}{C_D}(W_f^{0.5} - W_i^{0.5}) \rightarrow R \propto \frac{C_L^{0.5}}{C_D} \tag{14}$$

Figs. 18-20 show contours of vorticity magnitude for both models in the wingtip section in 3 different angles of attack containing 0º, 15º, and 20º. According to the figures, the vorticity structure is fully affected by the winglet, and the amount of the effects is based on the angle of attack. In fact, by incrementing the angle of attack from 0º to higher values, the area with high vorticity magnitude is propagated wider downstream of the wing. Also, winglet installation could affect more to reduce high-velocity gradients and enhance aerodynamic performance. According to Fig. 18, the winglet lessens the power of vortex cores downstream of the wing. Also, the winglet has caused vortex cores to propagate less in the control volume.

In the simple wing, local increment in vorticity magnitude leads to increasing the low-pressure area of the wing, as makes changes on the wing generated forces. Whiles blended wing decreases low-pressure areas where leads to significant enhancement on the wing aerodynamic locally and integrally. Fig. 19 confirms winglet effects on the wing's downstream area. In this figure, a positive angle of attack lets winglets affect the wing's lower surface and reduces high-vorticity area thickness. Also, for similar reasons, it does not affect the upper surface significantly. In Fig. 20, a 5º increment in the angle of attack makes mentioned observations more drastic. Besides, to reduce the thickness of the high-velocity area near the lower surface, it could separate into two parts. Also, it has more effects on the upper surface.

Fig. 21 shows the area-weighted average of vorticity magnitude on the wings at the section near the wingtip for various angles of attack. According to the figure, winglet installation causes a sensible effect on the vorticity magnitude value, whereas schematic trends are similar. This
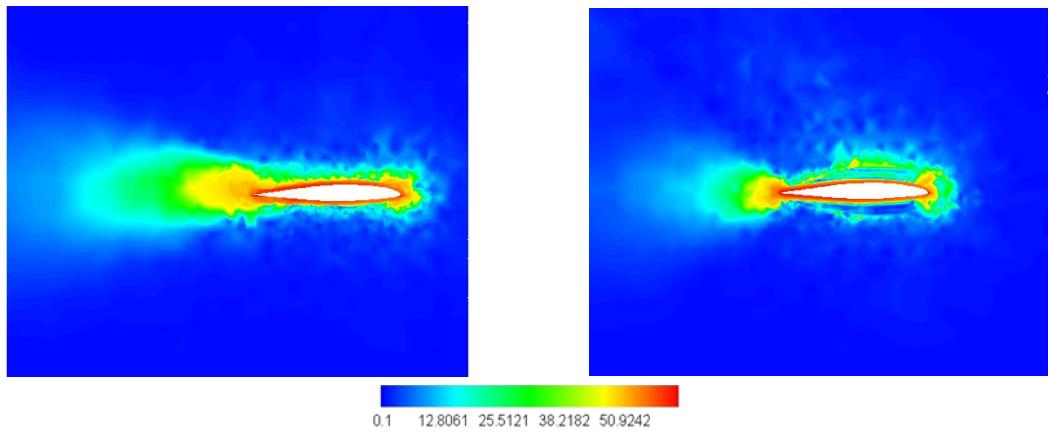
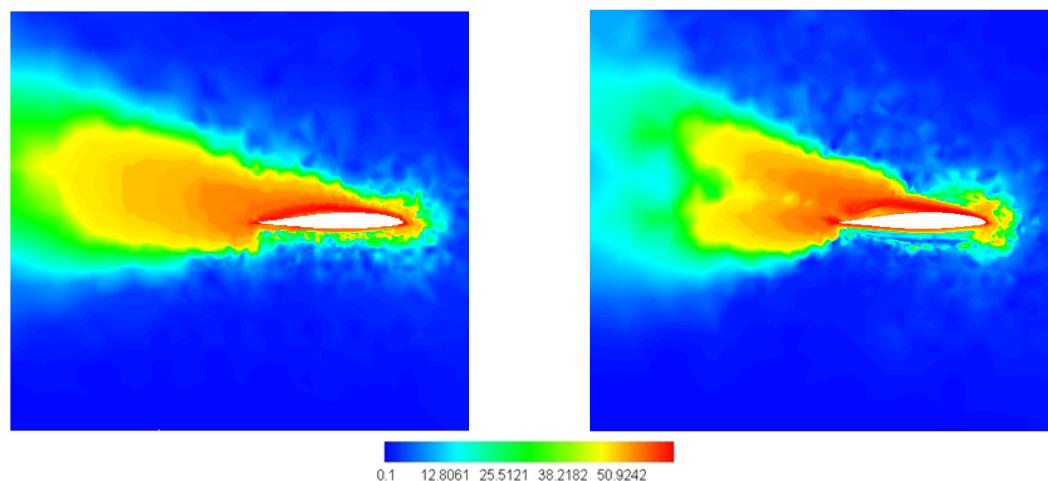Fig. 18 Contour of vorticity magnitude of simple (left) and blended wing (right) at α = 0º

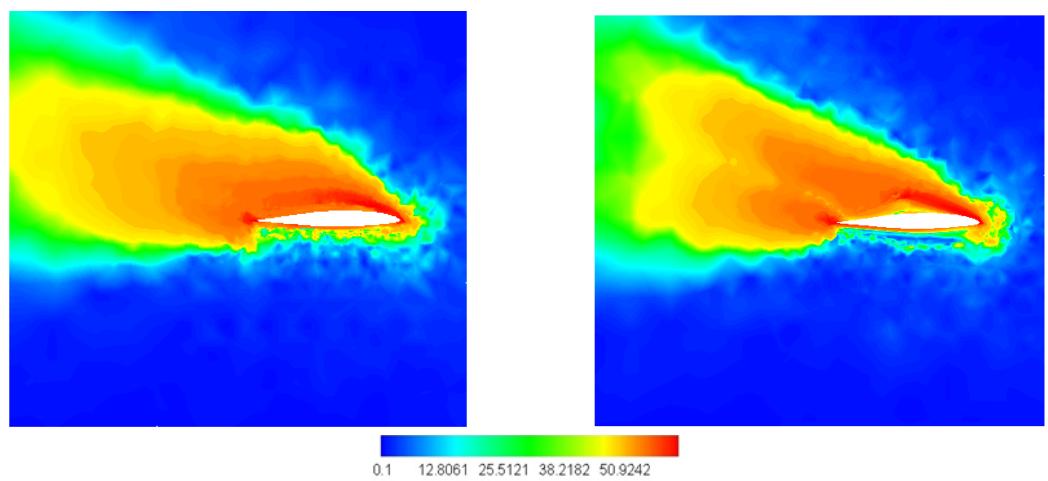Fig. 19 Contour of vorticity magnitude of simple (left) and blended wing (right) at α = 15º

Fig. 20 Contour of vorticity magnitude of simple (left) and blended wing (right) at α = 20º
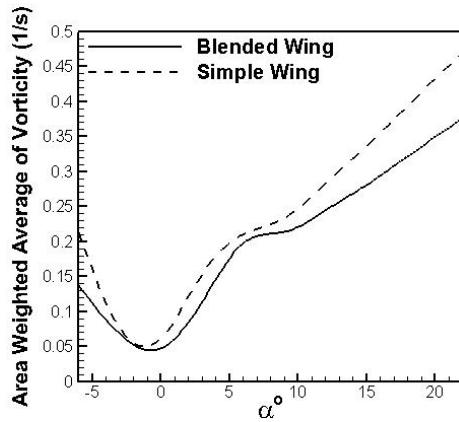
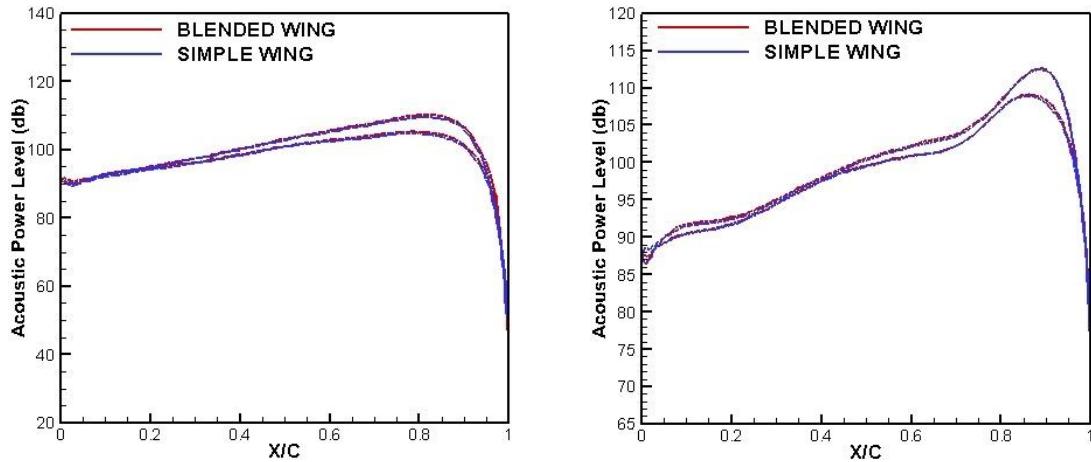Fig. 21 Area-weighted average of vorticity versus angle of attack

Fig. 22 Acoustic power level distribution on the sections with 2 (left) and 8 (right) distances from symmetry plane
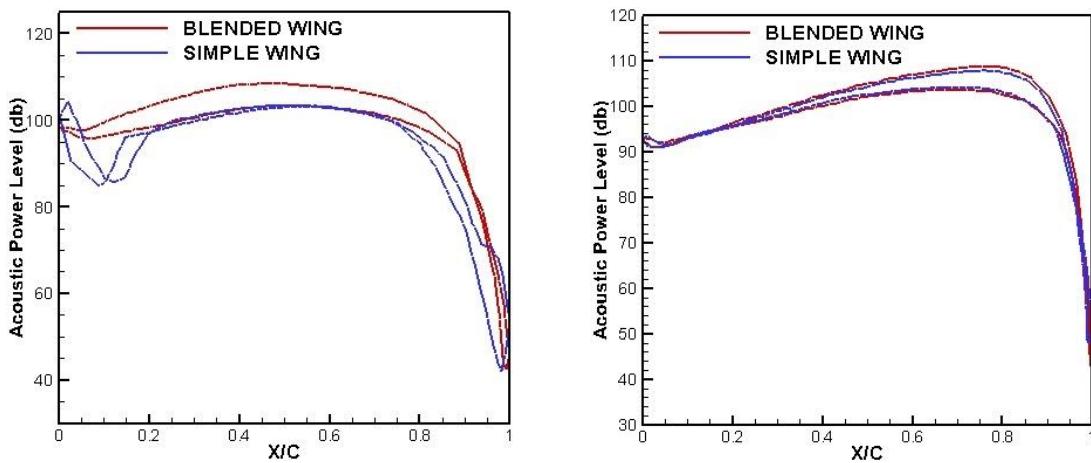

Fig. 23 Acoustic power level distribution on the sections with 12 (left) and 16.8 m (right) distances from symmetry plane

observation is more significant in higher angles of attack and less observable in the vicinity of 0º angle of attack. This is based on the natural increment of flow vorticity by increasing the angle of attack, which causes enhancement of flow turbulent features.

Figs. 22 and 23 show the acoustic power level distribution on the three sections on both wings. According to the figure, the winglet acoustic effects are more evident near the wingtip as well as the aerodynamics features. The dissipation of acoustic differences between the wings has occurred faster than pressure distribution differences by approaching the wing root from the wingtip. By examining the 1st and 2nd sections, it could be concluded that geometric changes affect the schematic distribution of pressure and acoustic power level. The wingtip section clarifies that winglet installation decreases generated noise at the leading edge area while increases acoustic parameters at the trailing edge.

Table 9 shows generated noise of trailing and leading edges of 3 similar sections on the simple and blended wings. According to Table 9, trailing edges produce more powerful noise than leading edges. This phenomenon is caused by more turbulent features and vorticity magnitude of the flow at the trailing edges. Also, the winglet has fewer effects at the trailing edges located in the wing root and middle sections, generated noise value nearly constant, and only in the wing tip section, a 6.75% difference is observable. On the other hand, the winglet affects generated noise by mentioned sections with difference percentages varying from 4.19% to 7.35%.

Table 10 illustrates the integral value of acoustic power level on simple and blended wings. According to the table, this parameter increases by 3.39% by winglet installation. Also cited in Fig. 5, the increment happens near the wingtip area and does not significantly affect the wing root. Table 11 shows wing acoustic power level value for various Mach numbers in the subsonic fluid flow regime. The table shows that Mach number increment affects acoustic power levels but keeps their difference percentage constant which means the winglet installation effect is independent of the Mach number value in subsonic flow.

Table 12 shows the acoustic power level downstream of the wingtip trailing edges. According to the table, the winglet increases noise in similar points downstream of the wing and delays noise-damping distance. That means in similar flights; the blended wing produces more noise than the simple model in a wider area.

Table 9 Acoustic power level value of trailing and leading edge on three sections

Distance from Symmetry Plane (m)	Position	Simple wing (dB)	Blended wing (dB)
2	Trailing-Edge	88.56	88.23
	Leading Edge	74.47	71.34
8.5	Trailing-Edge	90.22	91.32
	Leading Edge	57.87	43.81
16.8	Trailing-Edge	97.48	104.53
	Leading Edge	42.04	38.95

Table 10 Total acoustic power level value on simple and blended wing

Wing type	Value (dB)
Simple	12411.4
Blended	12847.4

Table 11 Total acoustic power level of the wings for various mach numbers

Mach number	Simple wing (dB)	Blended wing (dB)	Difference (%)
0.3	9544.3	9881.9	3.416%
0.4	10725.6	11102.4	3.394%
0.5	11348.1	12057.1	3.392%
0.6	1244.4	12847.4	3.393%
0.7	13074.2	13532.7	3.388%
0.785	13591.5	14068.2	3.389%

Table 12 Acoustic power level value for various points behind the wingtip trailing edge

Distance from symmetry plane (m)	Simple wing (dB)	Blended wing (dB)
0	97.483	104.531
0.285	45.268	52.793
0.785	30.374	34.528
1.285	24.505	19.682
1.785	12.589	19.572
2.285	11.968	14.145
2.785	6.322	10.416
3.285	3.954	9.308
3.785	2.615	7.552
4.285	0	5.2
4.785	0	4.171
5.285	0	3.19
5.785	0	1.927
6.285	0	1.424
6.385	0	0.513
6.785	0	0

Generally, research clears that winglet affects the aerodynamic and aeroacoustic performance of the wing reversely. On the other hand, the winglet enhances aerodynamic efficiency by increasing the lift force and decreasing the drag force and also increasing the wing's noise in terms of value and propagation power. According to the higher pressure turbulence of the blended wing compared with the simple, especially the wingtip area, generated acoustic waves increases dramatically. Also, according to the pressure difference increment of the lower and upper surfaces, the wing lift force increases and improves the wing's efficiency.

5. Conclusions

This paper investigated fluid flow around a simple and blended wing to study design change effects on aerodynamic and aeroacoustic efficiency. For this purpose, numerical simulation was used to solve the compressible fluid flow equations with consideration of turbulence. Also, to

achieve accurate results, a hybrid computational grid was generated around the models. According to the performance analysis of the simple and blended wing, the below results have been inferred:

• The static pressure coefficient distribution has conformity in various sections on the wings. Only in sections near the wingtip differences are observable, which causes improvements in the wing's aerodynamic performance. Generally, winglets improved a 3.78% flight range by increasing lift force and reducing drag force, which led to saving fuel consumption and maximizing payload.

• The acoustic performance of the wing is also dependent on the winglet. Winglet installation increased the generated noise of the wing surface by 3.39%, which a significant part related to the wingtip area.

• The increment of the generated noise value is independent of the flow Mach number. Thus, simulations reveal that the Mach number value between 0.3 and 0.785, the difference percentage of acoustic power level for the wings is constant.

•Also, the generated noise of the blended wing is more powerful and propagated in a broader area downstream of the wing. So, despite the winglet's aerodynamic enhancement, generated noise of the wing increased, which is a disadvantage for the winglet devices.

References

Abdelghany, E.S., Khalil, E.E., Abdellatif, O.E. and Elhariry, G. (2016), "Aircraft winglet design and performance: Cant angle effect", *Proceedings of the 14th International Energy Conversion Engineering Conference*, Salt Lake City, U.S.A., October.

Ali, A.H. (2020), "Aerodynamic characteristics comparison between spiroid and blended winglets", *J. Eng.*, **26**, 33-46. https://doi.org/10.31026/j.eng.2020.04.03.

Ansys Inc. (2011), "Ansys fluent theory guide", **15317**, 724-746, *ANSYS Inc.*, *USA*.

Azlin, M.A., Taib, C.M., Kasolang, S. and Muhammad, F. (2011), "CFD analysis of winglets at low subsonic flow", *Proceedings of the World Congress on Engineering*, London, U.K., July.

Brocklehurst, A. and Barakos, G. (2013), "A review of helicopter rotor blade tip shapes", *Prog. Aerosp. Sci.*, **56**, 35-74. https://doi.org/10.1016/j.paerosci.2012.06.003.

Chae, S., Yee, K., Yang, C., Aoyama, T., Jeong, S. and Obayashi, S. (2010), "Helicopter rotor shape optimization for the improvement of aeroacoustic performance in hover", *J. Aircr.*, **47**(5), 1770-1783. https://doi.org/10.2514/1.C000283.

Czech, M.J., Thomas, R.H. and Elkoby, R. (2012), "Propulsion airframe aeroacoustic integration effects for a hybrid wing body aircraft configuration", *Int. J. Aeroacoust.*, **11**(3-4), 335-367. https://doi.org/10.1260/1475-472X.11.3-4.335.

Diskin, B. and Thomas, J.L. (2016), "Introduction: Evaluation of RANS solvers on benchmark aerodynamic flows", *Am. Inst. Aeronaut. Astronaut.*, **54**, 2561-2576. https://doi.org/10.2514/1.J054642.

Dziubinski, A., Jaskowski, P. and Seredyn, T. (2016), "CFD analysis of agricultural aircraft aerodynamic characteristics", *Prace Instytutu Lotnictwa*, **4**, 312-337. https://doi.org/10.5604/05096669.1229486.

Eguea, J.P., Da silva, G.P.G. and Catalano, F.M. (2020), "Fuel efficiency improvement on a business jet using a camber morphing winglet concept", *Aerosp. Sci. Technol.*, **96**, 105542. https://doi.org/10.1016/j.ast.2019.105542.

Elham, A. and Van tooren, M.J. (2014), "Winglet multi-objective shape optimization", *Aerosp. Sci. Technol.*, **37**, 93-109. https://doi.org/10.1016/j.ast.2014.05.011.

Ewert, R., Dierke, J., Siebert, J., Neifeld, A., Appel, C., Siefert, M. and Kornow, O. (2011), "CAA broadband noise prediction for aeroacoustic design", *J. Sound Vib.*, **330**(17), 4139-4160. https://doi.org/10.1016/j.jsv.2011.04.014.

Farhan, A., Hassanpour, A., Burns, A. and Motlagh, Y.G. (2019), "Numerical study of effect of winglet

planform and airfoil on a horizontal axis wind turbine performance", *Renew. Energ.*, **131**, 1255-1273. https://doi.org/10.1016/j.renene.2018.08.017.

Fillola, G., Le pape, M.C. and Montagnac, M. (2004), "Numerical simulations around wing control surfaces", *Proceedings of the 24th International Congress of the Aeronautical Sciences*, Yokohama, Japan, August.

Gao, H., Zhu, W., Liu, Y. and Yan, Y. (2019), "Effect of various winglets on the performance of marine propeller", *Appl. Ocean Res.*, **86**, 246-256. https://doi.org/10.1016/j.apor.2019.03.006.

Gavrilovic, N.N., Rasuo, B.P., Dulikravich, G.S. and Parezanovic, V.B. (2015), "Commercial aircraft performance improvement using winglets", *FME Transact.*, **43**(1), 1-8. https://doi.org/10.5937/fmet1501001G.

Ghoreyshi, M., Vallespin, D., Da Ronch, A., Badcock, K., Vos, J. and Hitzel, S. (2010), "Simulation of aircraft manoeuvres based on computational fluid dynamics", *Proceedings of AIAA Atmospheric Flight Mechanics Conference*, Toronto, Canada, August.

Guerrero, J.E., Sanguineti, M. and Wittkowski, K. (2020), "Variable cant angle winglets for improvement of aircraft flight performance", *Meccanica*, **55**(10), 1917-1947. https://doi.org/10.1007/s11012-020-01230-1.

Hasanzadeh, K., Laurenseau, E., Saeed, F. and Paraschivoiu, I. (2012), "Wing aerodynamic performance analysis and stall prediction using canice2d-ns icing code", *Proceedings of the 20th Annual Conference of the CFD Society of Canada*, Grapevine, Canada, January.

Helal, H.S., Khalil, E.E., Abdellatif, O.E. and Elhariry, G.M. (2016), "Aerodynamic analyses of aircraft-blended winglet performance", *IOSR J. Mech. Civ. Eng. Ver*, **13**(13), 2320-2334. https://doi.org/10.9790/1684-1303046572.

Hiremath, S. and Malipatil, A.S. (2014), "CFD simulations of aircraft body with different angle of attack and velocity", *Int. J. Innov. Res. Sci. Eng. Technol.*, **3**(10), 16965-16972. https://doi.org/10.15680/IJIRSET.2014.0310077.

Horvath, C. and Vad, J. (2009), "Broadband noise source model acoustical investigation on unskewed and skewed axial flow fan cascades", *Proceedings of the 14th International Conference on Fluid Flow Technologies*, Budapest, Hungary, September.

Imamura, T., Hirai, T., Amemiya, K., Yokokawa, Y., Enomoto, S. and Yamamoto, K. (2010), "Aerodynamic and aeroacoustic simulations of a two-wheel landing gear", *Procedia Eng.*, **6**, 293-302. https://doi.org/10.1016/j.proeng.2010.09.031.

Jain, R., Jain, M.S. and Bajpai, L. (2016), "Aerodynamics of winglet: A computational fluid dynamics study using fluent", *Int. Res. J. Eng. Technol.*, **3**(6), 250-254. http://doi.org/10.13140/RG.2.2.35908.48009.

Jameson, A. and Fatica, M. (2006), "Using computational fluid dynamics for aerodynamics-a critical assessment", *Proceedings of the 23rd International Congress of Aeronautical Sciences*, Toronto, Canada, September.

Kobayashi, H., Yaji, K., Yamasaki, S. and Fujita, K. (2019), "Freeform winglet design of fin-and-tube heat exchangers guided by topology optimization", *Appl. Therm. Eng.*, **161**, 114020. https://doi.org/10.1016/j.applthermaleng.2019.114020.

Lazim, T.M., Mat, S. and Saint, H.Y. (2003), "Computational fluid dynamic simulation (CFD) and experimental study on wing-external store aerodynamic interference of a subsonic fighter aircraft", *Acta Polytechnica*, **43**(5). https://doi.org/10.14311/484.

Lefebvre, T., Canard-caruana, S., Le Tallec, C., David, F. and Neuville, N. (2010), "ANIBAL: A new aero-acoustic optimized propeller for light aircraft applications", *Proceedings of the 9th AIAA Aviation Technology, Integration, and Operations Conference (ATIO) and Aircraft Noise and Emissions Reduction Symposium (ANERS)*, Hilton Head, U.S.A., September.

Lefebvre, T., Canard–caruana, S., Le Tallec, C., David, F. and Neuville, N. (2010), "An overview of the ANIBAL project: a new low-noise and efficient propeller for light aircraft applications", *Proceedings of the 9th AIAA Aviation Technology, Integration, and Operations Conference (ATIO) and Aircraft Noise and Emissions Reduction Symposium (ANERS)*, Hilton head, U.S.A., September.

Li, H.B., Sun, Z.L and Peng, X. (2010), "Turbocharger noise prediction using broadband noise source model", *J. Beijing Inst. Technol.*, **19**(3), 312-317.

Mahmoudi, J.P. and Khodaparast, M. (2012), "Simulation of sound generated from outlet nozzle jet of an aircraft engine on the aircraft fuselage", *Proceedings of the 3rd International Conference on Acoustics and Vibrations*, Tehran, Iran, January.

Moayedi, A.M.M. (2016), "Numerical simulation of flow field around re-entry capsule and angle of attacks effect on flow structure", *Proceedings of the 1st International Conference on Mechanical and Aerospace Engineering*, Tehran, Iran, March.

Mahmood, C.A. and Das, R.K. (2019), "Performance comparison of different winglets by CFD", *Proceedings of the 2019 AIP Conference*, **2121**(1), 060006. AIP Publishing LLC. https://doi.org/10.1063/1.5115907.

Maughmer, M.D., Swan, T.S. and Willits, S.M. (2002), "Design and testing of a winglet airfoil for low-speed aircraft", *J. Aircr.*, **39**(4), 654-661. https://doi.org/10.2514/2.2978.

Minelli, G., Yao, H.D., Andersson, N., Hostmad, P., Forssen, J. and Krajnovic, S. (2020), "An aeroacoustic study of the flow surrounding the front of a simplified ICE3 high-speed train model", *Appl. Acoust.*, **160**, 107-125. https://doi.org/10.1016/j.apacoust.2019.107125.

Moayedi, M. and Mohammad, M.A. (2019), "Numerical simulation of flow field around space reentry capsule and studying the effects of angle of attack variations on flow structure", *J. Technol. Aerosp. Eng.*, **3**(1), 13-19.

Mohamud, O.M. and Johnson, P. (2006), "Broadband noise source models as aeroacoustic tools in designing low NVH HVAC ducts", *SAE Technical Paper*, 2006-01-1192, 2006. https://doi.org/10.4271/2006-01-1192.

Myilsamy, D., Thirumalay, Y. and Premkumar, P. (2015), "Performance Investigation of an Aircraft Wing at Various Cant Angle of Winglet Using CFD Simulation", *Proceedings of the 11th Altair Technology Conference India*, Bangalore, India, July.

Nardari, C., Casalino, D., Polidoro, F., Coralic, V., Lew, P.T. and Brodie, J. (2019), "Numerical and experimental investigation of flow confinement effects on UAV rotor noise", *Proceedings of the 25th AIAA/CEAS Aeroacoustics Conf*, Delft, Netherlands, May.

Ortiz, A.D., Quiroz, L.E. and Kock, R.A. (2002), "Aerodynamic performance analysis of a low-speed acrobatic airplane by numerical simulation", *Mecánica Computacional*, **1**, 378-391.

Pagano, A., Federico, L., Barbarino, M., Guida, F. and Aversano, M. (2008), "Multi-objective aeroacoustic optimization of an aircraft propeller", *Proceedings of the 12th AIAA/ISSMO Multidisciplinary Analysis and Optimization Conference*, Victoria, Canada, September.

Page, M. (2000), "Aerodynamic design of the Eagle E997 champ car", *Proceedings of the 18th Applied Aerodynamics Conference*, Denver, U.S.A., August. https://doi.org/10.2514/6.2000-4337.

Park, M.A., Barral, N., Ibanez, D., Kamentskiy, D.S., Krakos, J.A., Michal, T.R. and Loseille, A. (2018), "Unstructured grid adaptation and solver technology for turbulent flows", *Proceedings of the 2018 AIAA Aerospace Sciences Meeting*, Kissimmee, U.S.A., January.

Pietroniro, A.G., Mihaescu, M., Abom, M. and Knutsson, M. (2018), "A steady-state based investigation of automotive turbocharger compressor noise", *SAE Technical Paper*, 2018-01-1528, 2018. https://doi.org/10.4271/2018-01-1528.

Rubbert, P. (1990), "The impact of supercomputers on CFD", *Comput. Syst. Eng.*, **1**(1), 1-6. https://doi.org/10.1016/0956-0521(90)90043-K.

Sadraey, M.H. (2012), *Aircraft Design: A Systems Engineering Approach*, John Wiley & Sons, U.S.A.

Shankara, P. and Snyder, D. (2012), "Numerical simulation of high lift trap wing using STAR-CCM+", *Proceedings of the 30th AIAA Applied Aerodynamics Conference*, New Orleans, U.S.A., June.

Skinner, S.N. and Zare-behtash, H. (2018), "State-of-the-art in aerodynamic shape optimisation methods", *Appl. Soft Comput.*, **62**, 933-962. https://doi.org/10.1016/j.asoc.2017.09.030.

Tam, C.K. (1995), "Computational aeroacoustics-Issues and methods", *AIAA J.*, **33**(10), 1788-1796. https://doi.org/10.2514/3.12728.

Tinoco, E.N. (2007), "CFD uncertainty and validation for commercial aircraft applications", *NATO Symposium AVT*, **147**, 1-36.

Triet, N.M., Viet, N.N. and Thang, P.M. (2015). "Aerodynamic analysis of aircraft wing", *VNU J. Sci. Math.*

Phys., **31**(2).

Tsai, C.H., Fu, L.M., Tai, C.H., Huang, Y.L. and Leong, J.C. (2009), "Computational aero-acoustic analysis of a car with a rear spoiler", *Appl. Math. Model.*, **33**(9), 3661-73. https://doi.org/10.1016/j.apm.2008.12.004.

Wilcox, D.C. (1998), *Turbulence Modeling For CFD*, DCW industries La Canada, Canada.

Ye, X., Li, P., Li, C. and Ding, X. (2015), "Numerical investigation of blade tip grooving effect on performance and dynamics of an axial flow fan", *Energy*, **82**, 556-569. https://doi.org/10.1016/j.energy.2015.01.065.

Yoon, D.H., Kohama, Y. and Kato, T. (2003), "Wing-wing flow interaction of the aero-train", *Proceedings of the 56th Annual Meeting of the APS Division of Fluid Dynamics Invited Talks*, **56**, MM-006, New Jersey, U.S.A., November.

Zhang, L., Dongli, M., Muqing, Y. and Shaoqi, W. (2020), "Optimization and analysis of winglet configuration for solar aircraft", *Chinese J. Aeronaut.*, **33**(12), 3238-3252. https://doi.org/10.1016/j.cja.2020.04.008.

GY